STRUCTURAL CHEMISTRY

ISSN 2053-2296

Single-crystal structure determination of psilocybin after dehydration

Sonya K. Emmett,[a] Lee Cameron,[a] Mark Hestermann,[b] Darren Holland,[a] Simon Kessler,[a] Luke McFarlane,[b] Yit-Heng Chooi[a] and Stephen A. Moggach[a]*

[a]School of Molecular Sciences, The University of Western Australia, Perth, WA 6009, Australia, and [b]Natural MedTech, Melbourne, VIC 3146, Australia. *Correspondence e-mail: stephen.moggach@uwa.edu.au

Received 15 June 2026
Accepted 27 July 2026

Edited by I. Oswald, University of Strathclyde, United Kingdom

Keywords: crystal structure; psilocybin; phase elucidation; anhydrous; phosphate; psychoactive compound; polymorphs.

CCDC references: 2562278; 2562279

Supporting information: this article has supporting information at journals.iucr.org/c

The crystal structure of the known low-temperature anhydrous phase of psilocybin {3-[2-(dimethylamino)ethyl]-1*H*-indol-4-yl dihydrogen phosphate, $C_{12}H_{17}N_2O_4P$} is reported. While the structure was previously characterized using powder X-ray diffraction, this study describes the first determination *via* single-crystal X-ray diffraction. High-resolution structural models were obtained both before and after *in situ* dehydration, allowing for a direct comparison of the lattice response to water loss.

1. Introduction

Found as a natural product in various mushrooms around the world, *psilocybin* is a phosphorylated tryptamine derivative that undergoes dephosphorylation within the human body to produce the psychoactive compound *psilocin* (Fig. 1) (Tylš *et al.*, 2014). The therapeutic properties of psilocybin have attracted renewed interest in the medical field in the last two decades due to an observed efficacy in the treatment of psychiatric and substance abuse disorders, including post-traumatic stress disorder, treatment resistant depression, anxiety and addiction to nicotine and alcohol (Bogenschutz *et al.*, 2015; Johnson *et al.*, 2014).

Psilocybin has been reported previously with two anhydrous phases, one trihydrate, six solvates and one cocrystal (Table 1) (Sherwood *et al.*, 2022). After the drug's first synthesis in 1958 (Hofmann *et al.*, 1958), the anhydrous form of psilocybin was first reported from separately dried trihydrate and methanolate solvates in 1976, and confirmed with IR spectroscopy and differential scanning calorimetry (DSC) (Kuhnert-Brandstätter & Heindl, 1976). The hygroscopic nature of psilocybin was also observed in this study, and the authors noted that transitions between the hydrous and anhydrous forms could occur depending on environmental factors such as humidity and temperature.

The first and second anhydrous phases of psilocybin were noted in 2018 under a patent application by Compass Pathways (Londesbrough *et al.*, 2019). These were labelled as *Polymorph A′* (the first lower-temperature anhydrate) and *Polymorph B* (a second higher-temperature anhydrate), and were reported using powder X-ray diffraction (PXRD). A third patent was lodged under the label *Polymorph A* as a 'novel isostructural variant'. In 2022, *Polymorph A* was shown by Sherwood *et al.* (2022) to be a mixed material of *Polymorph A′* and *Polymorph B* rather than a new phase.

While structure solution with single-crystal X-ray diffraction (SCXRD) has been successfully carried out for many of psilocybin's solvates, poor crystal quality or small crystal size

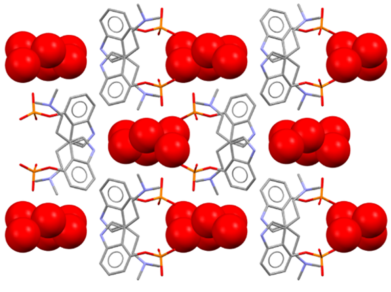

Table 1
Reported phases of anhydrous psilocybin and precursor solvates, and method of characterization.

	SCXRD	PXRD	DSC	IR
Methanol solvate (2:1 *v*/*v*)	Weber & Petcher (1974)	Greenan *et al.* (2020)	Kuhnert-Brandstätter & Heindl (1976)	Kuhnert-Brandstätter & Heindl (1976)
Trihydrate	Greenan *et al.* (2020)	Greenan *et al.* (2020) and Sherwood *et al.* (2022)	Kuhnert-Brandstätter & Heindl (1976)	Kuhnert-Brandstätter & Heindl (1976)
First anhydrate/*Polymorph A′*	–	Greenan *et al.* (2020)†	Kuhnert-Brandstätter & Heindl (1976)	Hofmann *et al.* (1958) and Kuhnert-Brandstätter & Heindl (1976)
Second anhydrate/*Polymorph B*	–	Greenan *et al.* (2020), Londesbrough *et al.* (2019), Sherwood *et al.* (2022) and Kargbo *et al.* (2022)	Greenan *et al.* (2020)	–

† High-resolution PXRD was used to generate a structure solution.

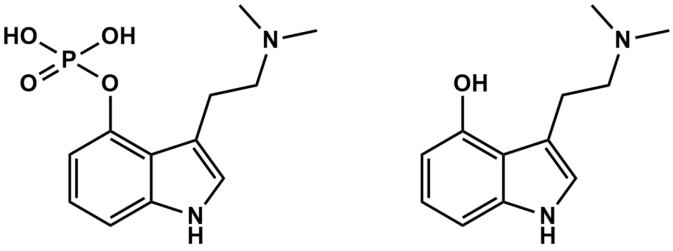

Figure 1
Chemical structure of psilocybin (left) and psilocin (right).

due to mechanical fracturing during dehydration is cited as a significant issue preventing the same being done for anhydrous psilocybin. The structures of *Polymorph A′* and *Polymorph B* were solved at 295 K from high-resolution PXRD patterns in 2022, but SCXRD data of either psilocybin anhydrate phase have been unavailable (Sherwood *et al.*, 2022). In the present study, psilocybin obtained *via* biosynthetic production using an engineered yeast system was used as the starting material for crystallization and structure analysis, providing access to material suitable for single-crystal analysis. With this in mind, herein we describe the dehydration protocol and first SCXRD structure of the anhydrous *Polymorph A′* form of psilocybin. *Polymorph A′* is the crystalline anhydrate that first forms during the drying process, and changes in partial trace amounts into *Polymorph B* upon drying at ambient pressures above 38–40 °C (Kargbo *et al.*, 2022; Greenan *et al.*, 2020). *Polymorph A′* is converted to the higher-temperature phase in totality above 160 °C.

2. Experimental

2.1. Sample preparation

A two-step drying process was used to obtain crystals of only *Polymorph A′*, following the method outlined by Sherwood *et al.* (2022). A sample of psilocybin was provided by Natural MedTech and recrystallized from water at 60 °C, then

Table 2
Experimental details.

For both determionations: orthorhombic, *Pbca*, Z = 8. Experiments were carried out at 100 K with Cu $K\alpha$ radiation using a Rigaku XtaLAB Synergy diffractometer with a HyPix detector. Absorption was corrected for by multi-scan methods (*CrysAlis PRO*; Rigaku OD, 2024). H-atom parameters were constrained.

	Dehydrated psilocybin	Psilocybin trihydrate
Crystal data		
Chemical formula	$C_{12}H_{17}N_2O_4P$	$C_{12}H_{17}N_2O_4P{\cdot}3H_2O$
M_r	284.24	338.29
a, b, c (Å)	15.920 (3), 9.322 (3), 17.466 (5)	14.3405 (6), 8.2707 (3), 27.098 (1)
V (Å^3)	2592.1 (11)	3214.0 (2)
μ (mm^{-1})	2.02	1.85
Crystal size (mm)	0.23 × 0.15 × 0.11	0.13 × 0.05 × 0.04
Data collection		
T_{min}, T_{max}	0.210, 1.000	0.615, 1.000
No. of measured, independent and observed [$I > 2\sigma(I)$] reflections	4440, 1013, 486	12268, 3256, 2382
R_{int}	0.121	0.091
θ_{max} (°)	45.0	79.3
(sin $\theta/\lambda)_{max}$ (Å^{-1})	0.458	0.637
Refinement		
$R[F^2 > 2\sigma(F^2)]$, $wR(F^2)$, S	0.082, 0.280, 1.04	0.052, 0.120, 1.04
No. of reflections	1013	3256
No. of parameters	176	211
$\Delta\rho_{max}$, $\Delta\rho_{min}$ (e Å^{-3})	0.32, −0.39	0.36, −0.48

Computer programs: *CrysAlis PRO* (Rigaku OD, 2024), *SHELXT2018* (Sheldrick, 2015*a*), *SHELXL2019* (Sheldrick, 2015*b*) and *OLEX2* (Dolomanov *et al.*, 2009).

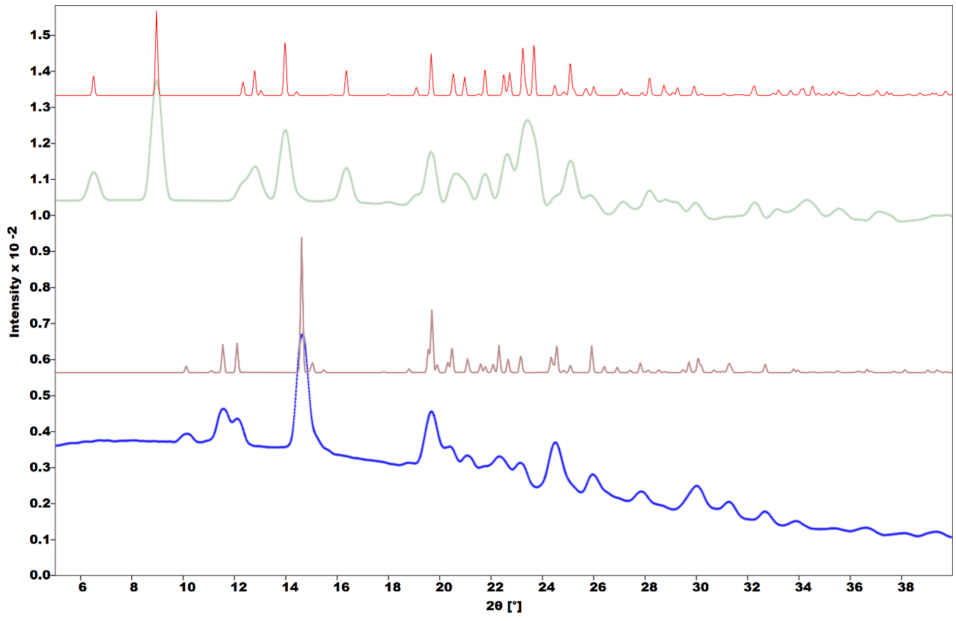

Figure 2
Comparison of the PXRD patterns for psilocybin trihydrate and *Polymorph A′*. The experimental patterns (green for the trihydrate and blue for *Polymorph A′*) are shown alongside their respective calculated patterns derived from SCXRD data (red for the trihydrate and grey for *Polymorph A′*) for structural validation.

dried under vacuum for 24 h at temperatures between 35 and 45 °C. A subsample of these hydrated crystals was removed for analysis, and the remaining crystals were then dried under vacuum for a further 24 h in the temperature range 50–60 °C. PXRD data were collected under ambient temperature conditions on both the hydrated subsample and the dehydrated sample to screen the phase composition of the bulk material. PXRD data were collected on sub- to micron-sized crystals on a Synergy-S diffractometer in transmission geometry, which confirmed the first-step subsample and final two-step product as predominantly psilocybin trihydrate and *Polymorph A′*, respectively (Fig. 2).

2.2. SCXRD structure solution and refinement details

The particle size distribution of the original sample was significant, with sub-to micron-sized crystals, as well as several crystallites of 50 µm and bigger. SCXRD data were collected on these larger crystals from the bulk samples. Data collection was conducted at 100 K on the recrystallized hydrate phase

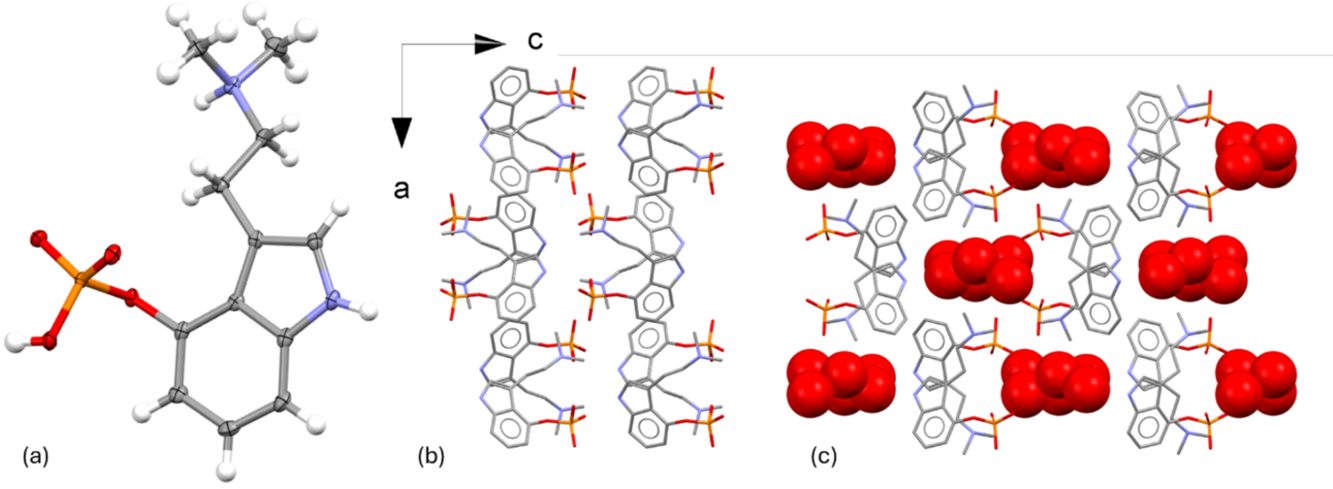

Figure 3
(*a*) The molecular connectivity of psilocybin (taken from the trihydrate crystal structure), with displacement ellipsoids drawn at the 50% probability level. Colour code: C grey, H white, N blue, O red and P orange. Crystal packing of (*b*) the anhydrous *Polymorph A′* and (*c*) the trihydrate form, both viewed down the *b* axis. Molecules are shown in stick representation, with the exception of the water O atoms in the trihydrate, which are rendered as red space-filling spheres to highlight their positions within the channels. Note the significant contraction of the unit cell along the *c* axis upon dehydration, corresponding to the collapse of the lattice into the anhydrous phase.

Table 3
Unit-cell dimensions for *Polymorph A′* from published powder (PXRD) and our own single-crystal data (SCXRD), transformed for comparison.

	Polymorph A′ (PXRD)	*Polymorph A′* (SCXRD)
CCDC refcode	TAVZID	n/a
Temperature (K)	295	100
a (Å)	17.4979 (2)	17.466 (5)
b (Å)	16.0914 (1)	15.920 (3)
c (Å)	9.34815 (7)	9.322 (3)
Volume (Å^3)	2632.11 (3)	2592.1 (11)

and on a separate crystal from the post heated and dried sample. Relevant crystallographic information is provided in Table 2.

On initial inspection, anhydrous *Polymorph A′* appeared subtely different to the reported anhydrous phase of Sherwood *et al.* (2022) due to a transformation of the unit-cell dimensions. In order to compare with the published structure [Cambridge Structural Database (CSD; Groom *et al.*, 2016) refcode TAVZID], we transformed the unit-cell dimensions by applying the following matrix:

$$\begin{pmatrix} 0 & 0 & 1 \\ -1 & 0 & 0 \\ 0 & -1 & 0 \end{pmatrix}$$

3. Results and discussion

During the first step, psilocybin trihydrate crystallized in the orthorhombic space group *Pbca*, with water-filled channels parallel to the *b* axis stabilized by hydrogen bonding to the phosphate moieties (Fig. 3 and Fig. S1 in the supporting information). During the initial stage of dehydration, thermal or vacuum driving forces induce the rapid loss of water molecules occupying the 22.7% void volume (729.7 Å^3) within the one-dimensional channels running parallel to the *b* axis. This loss breaks the critical host–guest hydrogen bonds stabilizing the phosphate moieties, leaving unsupported cylindrical cavities within the lattice. Deprived of solvent support, these channels collapse inward along the transverse crystal directions, causing a large contraction along the *c*-axis direction [with a reduction from 27.0980 (10) to 17.466 (5) Å]. To optimize space-filling in the absence of channel water, neighbouring stacks of zwitterionic psilocybin molecules undergo a co-operative shear-like sliding motion past one another, closing the macroscopic voids. When water evacuation occurs rapidly at the crystal exterior, localized channel collapse near the surface can seal off interior channels, creating trapped pockets of high-pressure water vapour. The combined localized strain from both side-chain deformation and trapped vapour pressure ultimately leads to micro-cracking and crystal fracturing, explaining the mechanically destructive nature of the dehydration transition. This structural reorganization drives a specific rearrangement of the hydrogen-bonding network. While the phosphate groups remain paired as a dimer and retain a direct hydrogen bond from the protonated dimethylammonium group in both phases, the loss of solvent causes the phosphate group to forfeit two hydrogen bonds with channel water. To compensate, the collapse allows the phosphate group to form a new direct N—H···O hydrogen bond with the indole N—H group – a contact that was strictly water-mediated prior to dehydration.

Comparison of this experimental trihydrate model with the previously reported structure reveals negligible structural disparity. A three-dimensional molecular overlay yields a root-mean-square deviation (RMSD) of 0.0121 Å and a maximum atomic displacement of 0.0280 Å, confirming that the atomic positions and molecular conformation in our structure are virtually identical to the published reference data (Arlin *et al.*, 2021).

Psilocybin anhydrate *Polymorph A′* crystallized in the orthorhombic space group *Pbca*, with a unit-cell volume of 2592.1 (11) Å^3 [Tables 2 and 3, and Fig. 3(*b*)]. The anhydrous psilocybin structure outlined herein is structurally analogous to Sherwood's prior solution, however, it has been re-indexed conventionally using the directionality insights provided by SCXRD. The indexing we use also makes it easier to compare the trihydrate and anhydrous *Polymorph A′* forms. The unit-cell dimensions we determined are marginally smaller, which is unsurprising considering that the data were collected at 100 K, whereas the original PXRD data were collected at room temperature (298 K).

Data for the anhydrous *Polymorph A′* could only be collected to 1 Å resolution without prohibitively long collection times. This is expected, as the loss of water results in a 19.35% reduction in the unit-cell volume. Notably, the successful collection of large intact crystals post-dehydration was a highlight of this study, as the rapid evacuation of water typically causes significant mechanical fracturing.

To quantitatively compare our single-crystal structure of anhydrous *Polymorph A′* with the literature, structural overlays were performed using *Mercury* (Macrae *et al.*, 2020). Our experimental SCXRD structure shows outstanding agreement with both the experimental powder structure reported by Sherwood and co-workers (RMSD = 0.082 Å; molecular overlay = 0.042 Å) and a VASP (Vienna Ab initio Simulation Package)-optimized DFT (density functional theory) model (RMSD = 0.090 Å; molecular overlay = 0.039 Å), which was reported in the same article. This remarkably low RMSD confirms that the single-crystal structure determination accurately captures the true anhydrous geometry. The *Mogul* (Bruno *et al.*, 2004) intramolecular geometry check highlights notable conformational differences in the dimethylaminoethyl side chain in the hydrated and anhydrous forms. Notably, in the trihydrate, the C—N—N—C torsion angles adopt expected values of approximately ≈65° and ≈−70°, corresponding to standard low-energy *gauche* preferences. In contrast, the experimental torsion angle in the anhydrous phase measures 86.8 and −149.7°, and falls directly into the low-frequency local minimum between these two main energy wells, further highlighting the torsional strain accommodated in the anhydrous crystal packing.

4. Conclusion

In summary, this study demonstrates that the dehydration of psilocybin trihydrate can be achieved through a controlled two-step vacuum-drying protocol. Despite the significant 19.35% reduction in unit-cell volume – driven by the collapse of water-filled channels – we have successfully reported the first single-crystal X-ray diffraction structure of an anhydrous psilocybin phase, denoted *Polymorph A′*. While dehydration is often considered a mechanically destructive process, this work confirms that large intact single crystals can be recovered and analyzed, overcoming previous limitations in structure characterization. These findings provide critical insights into the structural response of psilocybin to water loss and establish a foundation for further investigation into its various solid-state forms.

Acknowledgements

The authors thank the UWA XRD Facility for access to equipment and facilities.

Conflict of interest

LM and MH are employees of Natural MedTech.

Funding information

The following funding is acknowledged: Australian Research Council (Mid-Career Industry Fellowship IM230100154 to Yit-Heng Chooi).

References

Arlin, J.-B., Greenan, C., Lorimer, K., Kargbo, K. K. R., Meisenheimer, P., Tarpley, W. G. & Sherwood, A. (2021). CSD Communication: Cambridge Crystallographic Data Centre. CCDC deposition No. 2060128; CSD refcode TAVZUC.

Bogenschutz, M. P., Forcehimes, A. A., Pommy, J. A., Wilcox, C. E., Barbosa, P. C. & Strassman, R. J. (2015). *J. Psychopharmacol.* **29**, 289–299.

Bruno, I. J., Cole, J. C., Kessler, M., Luo, J., Motherwell, W. D. S., Purkis, D. C., Smith, B. R., Taylor, R., Cooper, R. I., Harris, S. E. & Orpen, A. G. (2004). *J. Chem. Inf. Comput. Sci.* **44**, 2133–2144.

Dolomanov, O. V., Bourhis, L. J., Gildea, R. J., Howard, J. A. K. & Puschmann, H. (2009). *J. Appl. Cryst.* **42**, 339–341.

Greenan, C., Arlin, J.-B., Lorimer, K., Kaylo, K., Kargbo, R., Meisenheimer, P., Tarpley, W. & Sherwood, A. (2020). *Preparation and Characterization of Novel Crystalline Solvates and Polymorphs of Psilocybin and Identification of Solid Forms Suitable for Clinical Development*. https://doi.org/10.13140/RG.2.2.32357.14560.

Groom, C. R., Bruno, I. J., Lightfoot, M. P. & Ward, S. C. (2016). *Acta Cryst.* B**72**, 171–179.

Hofmann, A., Frey, A., Ott, H., Petrzilka, Th. & Troxler, F. (1958). *Experientia* **14**, 397–399.

Johnson, M. W., Garcia-Romeu, A., Cosimano, M. P. & Griffiths, R. R. (2014). *J. Psychopharmacol.* **28**, 983–992.

Kargbo, R. B., Sherwood, A. M., Meisenheimer, P., Lenoch, K. & Abebe, S. (2022). *ACS Omega* **7**, 5429–5436.

Kuhnert-Brandstätter, M. & Heindl, W. (1976). *Arch. Pharm.* **309**, 625–631.

Londesbrough, D. J., Brown, C., Northen, J. S., Moore, G., Patil, H. K., Nichols, D. E. & Casale, R. T. (2019). US Patent Appl. No. US 2019/0112328 A1 (or WO Patent Publication No. WO 2019/081481 A1).

Macrae, C. F., Sovago, I., Cottrell, S. J., Galek, P. T. A., McCabe, P., Pidcock, E., Platings, M., Shields, G. P., Stevens, J. S., Towler, M. & Wood, P. A. (2020). *J. Appl. Cryst.* **53**, 226–235.

Rigaku OD (2024). *CrysAlis PRO*. Rigaku Oxford Diffraction Ltd, Yarnton, Oxfordshire, England.

Sheldrick, G. M. (2015*a*). *Acta Cryst.* A**71**, 3–8.

Sheldrick, G. M. (2015*b*). *Acta Cryst.* C**71**, 3–8.

Sherwood, A. M., Kargbo, R. B., Kaylo, K. W., Cozzi, N. V., Meisenheimer, P. & Kaduk, J. A. (2022). *Acta Cryst.* C**78**, 36–55.

Tylš, F., Páleníček, T. & Horáček, J. (2014). *Eur. Neuropsychopharmacol.* **24**, 342–356.

Weber, H. P. & Petcher, T. J. (1974). *J. Chem. Soc. Perkin Trans. 2* pp. 942–946.

supporting information

Acta Cryst. (2026). C**82** [https://doi.org/10.1107/S2053229626007692]

Single-crystal structure determination of psilocybin after dehydration

Sonya K. Emmett, Lee Cameron, Mark Hestermann, Darren Holland, Simon Kessler, Luke McFarlane, Yit-Heng Chooi and Stephen A. Moggach

Computing details

3-[2-(Dimethylamino)ethyl]-1*H*-indol-4-yl dihydrogen phosphate (ps1_recryst_dehydrated_100k_auto)

Crystal data

$C_{12}H_{17}N_2O_4P$
M_r = 284.24
Orthorhombic, *Pbca*
a = 15.920 (3) Å
b = 9.322 (3) Å
c = 17.466 (5) Å
V = 2592.1 (11) Å^3
Z = 8
F(000) = 1200
D_x = 1.457 Mg m^{-3}
Cu *Kα* radiation, *λ* = 1.54184 Å
Cell parameters from 618 reflections
θ = 5.0–41.9°
μ = 2.02 mm^{-1}
T = 100 K
Block, clear light colourless
0.23 × 0.15 × 0.11 mm

Data collection

XtaLAB Synergy, Single source at home/near, HyPix diffractometer
Radiation source: micro-focus sealed X-ray tube, PhotonJet (Cu) X-ray Source
Mirror monochromator
Detector resolution: 10.0000 pixels mm^{-1}
ω scans
Absorption correction: multi-scan (CrysAlis PRO; Rigaku OD, 2024)
T_{min} = 0.210, T_{max} = 1.000
4440 measured reflections
1013 independent reflections
486 reflections with $I > 2\sigma(I)$
R_{int} = 0.121
θ_{max} = 45.0°, θ_{min} = 5.1°
h = −14→14
k = −8→8
l = −15→15

Refinement

Refinement on F^2
Least-squares matrix: full
$R[F^2 > 2\sigma(F^2)]$ = 0.082
$wR(F^2)$ = 0.280
S = 1.04
1013 reflections
176 parameters
0 restraints
Hydrogen site location: inferred from neighbouring sites
H-atom parameters constrained
$w = 1/[\sigma^2(F_o^2) + (0.1635P)^2 + 1.9185P]$ where $P = (F_o^2 + 2F_c^2)/3$
$(\Delta/\sigma)_{max} < 0.001$
$\Delta\rho_{max}$ = 0.32 e Å^{-3}
$\Delta\rho_{min}$ = −0.39 e Å^{-3}
Extinction correction: SHELXL2019 (Sheldrick, 2015*b*), $Fc^* = kFc[1+0.001xFc^2\lambda^3/\sin(2\theta)]^{-1/4}$
Extinction coefficient: 0.0019 (7)

Special details

Geometry. All e.s.d.'s (except the e.s.d. in the dihedral angle between two l.s. planes) are estimated using the full covariance matrix. The cell e.s.d.'s are taken into account individually in the estimation of e.s.d.'s in distances, angles and torsion angles; correlations between e.s.d.'s in cell parameters are only used when they are defined by crystal symmetry. An approximate (isotropic) treatment of cell e.s.d.'s is used for estimating e.s.d.'s involving l.s. planes.

Refinement. Both structures were solved using the *SHELXT2018* (Sheldrick, 2015*a*) solution program using dual space methods and by using *OLEX2* (Dolomanov *et al.*, 2009) as the graphical interface. The models were refined with *SHELXL* (Sheldrick, 2015*b*) using full-matrix least-squares minimization on F^2.

Fractional atomic coordinates and isotropic or equivalent isotropic displacement parameters (Å²)

	x	*y*	*z*	U_{iso}*/U_{eq}
P1	0.4070 (3)	0.3707 (6)	0.4597 (2)	0.0944 (18)
O5	0.3983 (5)	0.4354 (11)	0.3742 (6)	0.089 (3)
O4	0.3807 (5)	0.5011 (12)	0.5083 (6)	0.097 (3)
H4	0.420908	0.559174	0.511170	0.146*
O2	0.3426 (6)	0.2545 (11)	0.4697 (5)	0.094 (3)
O3	0.4968 (5)	0.3250 (11)	0.4732 (5)	0.099 (3)
N6	0.3064 (10)	0.2954 (15)	0.1345 (7)	0.100 (4)
H6	0.303666	0.259823	0.087938	0.120*
N7	0.1439 (7)	0.4763 (14)	0.4261 (7)	0.092 (4)
H7	0.164342	0.577662	0.427131	0.110*
C15	0.2700 (10)	0.4150 (18)	0.2410 (11)	0.090 (5)
C8	0.4122 (13)	0.3516 (18)	0.3080 (10)	0.090 (5)
C9	0.3518 (11)	0.3522 (19)	0.2509 (10)	0.094 (5)
C17	0.1926 (9)	0.3964 (16)	0.3649 (8)	0.085 (4)
H17A	0.157565	0.316855	0.345110	0.102*
H17B	0.243571	0.353977	0.388161	0.102*
C11	0.4443 (13)	0.1969 (18)	0.1728 (10)	0.099 (5)
H11	0.454001	0.142511	0.127696	0.118*
C14	0.2444 (11)	0.3774 (19)	0.1686 (11)	0.092 (5)
H14	0.192529	0.403512	0.145631	0.110*
C16	0.2182 (9)	0.492 (2)	0.2988 (9)	0.107 (5)
H16A	0.167140	0.530261	0.273680	0.128*
H16B	0.250588	0.574701	0.318927	0.128*
C13	0.4886 (12)	0.2824 (19)	0.2994 (10)	0.095 (5)
H13	0.530983	0.289991	0.337457	0.114*
C18	0.1581 (10)	0.4131 (17)	0.5029 (8)	0.096 (5)
H18A	0.139113	0.313060	0.503053	0.144*
H18B	0.126387	0.467613	0.541220	0.144*
H18C	0.218078	0.416805	0.515245	0.144*
C19	0.0510 (9)	0.4782 (19)	0.4067 (8)	0.106 (6)
H19A	0.043959	0.491989	0.351406	0.160*
H19B	0.023550	0.556948	0.434153	0.160*
H19C	0.025443	0.386856	0.421847	0.160*
C12	0.5018 (10)	0.202 (2)	0.2339 (13)	0.105 (5)
H12	0.552047	0.147444	0.230079	0.126*
C10	0.3728 (12)	0.278 (2)	0.1840 (11)	0.096 (5)

Atomic displacement parameters (Å²)

	U^{11}	U^{22}	U^{33}	U^{12}	U^{13}	U^{23}
P1	0.077 (3)	0.111 (4)	0.094 (3)	0.002 (3)	0.005 (2)	−0.002 (3)
O5	0.078 (7)	0.114 (8)	0.074 (7)	−0.005 (6)	0.001 (5)	0.006 (7)
O4	0.071 (7)	0.124 (9)	0.097 (7)	−0.002 (6)	0.009 (6)	0.003 (7)
O2	0.077 (6)	0.116 (8)	0.089 (7)	0.004 (7)	0.004 (5)	0.009 (6)
O3	0.081 (7)	0.122 (9)	0.094 (8)	0.019 (6)	0.005 (6)	0.000 (6)
N6	0.086 (10)	0.124 (12)	0.089 (9)	−0.002 (9)	0.004 (10)	0.005 (9)
N7	0.069 (9)	0.115 (11)	0.091 (9)	0.000 (8)	−0.005 (7)	−0.004 (8)
C15	0.059 (12)	0.107 (14)	0.106 (15)	−0.001 (10)	0.000 (11)	−0.007 (11)
C8	0.097 (14)	0.084 (12)	0.088 (14)	0.000 (11)	0.004 (13)	−0.005 (10)
C9	0.089 (16)	0.121 (14)	0.072 (12)	0.000 (12)	0.001 (12)	−0.006 (11)
C17	0.086 (11)	0.079 (11)	0.090 (11)	0.001 (9)	−0.007 (9)	0.003 (10)
C11	0.096 (13)	0.091 (13)	0.109 (14)	0.002 (11)	0.007 (13)	0.003 (10)
C14	0.076 (11)	0.105 (13)	0.096 (13)	−0.008 (11)	−0.001 (11)	0.004 (11)
C16	0.083 (12)	0.140 (16)	0.097 (12)	0.012 (11)	−0.006 (9)	0.011 (12)
C13	0.092 (14)	0.100 (13)	0.093 (13)	−0.005 (12)	0.008 (10)	−0.005 (11)
C18	0.094 (11)	0.113 (13)	0.081 (10)	−0.010 (10)	0.002 (8)	0.003 (9)
C19	0.067 (11)	0.159 (17)	0.093 (11)	0.010 (11)	0.005 (8)	0.011 (10)
C12	0.076 (12)	0.125 (16)	0.114 (15)	0.016 (11)	0.004 (12)	0.014 (13)
C10	0.080 (13)	0.116 (15)	0.090 (14)	0.006 (12)	0.005 (12)	0.006 (12)

Geometric parameters (Å, º)

P1—O5	1.616 (10)	C17—H17A	0.9900
P1—O4	1.541 (10)	C17—H17B	0.9900
P1—O2	1.501 (10)	C17—C16	1.516 (19)
P1—O3	1.510 (9)	C11—H11	0.9500
O5—C8	1.413 (17)	C11—C12	1.41 (2)
O4—H4	0.8400	C11—C10	1.38 (2)
N6—H6	0.8800	C14—H14	0.9500
N6—C14	1.382 (17)	C16—H16A	0.9900
N6—C10	1.376 (17)	C16—H16B	0.9900
N7—H7	1.0000	C13—H13	0.9500
N7—C17	1.516 (16)	C13—C12	1.38 (2)
N7—C18	1.482 (15)	C18—H18A	0.9800
N7—C19	1.518 (16)	C18—H18B	0.9800
C15—C9	1.44 (2)	C18—H18C	0.9800
C15—C14	1.375 (18)	C19—H19A	0.9800
C15—C16	1.49 (2)	C19—H19B	0.9800
C8—C9	1.39 (2)	C19—H19C	0.9800
C8—C13	1.386 (19)	C12—H12	0.9500
C9—C10	1.40 (2)		
O4—P1—O5	101.1 (6)	C10—C11—H11	122.8
O2—P1—O5	108.6 (5)	C10—C11—C12	114.3 (17)
O2—P1—O4	108.6 (6)	N6—C14—H14	125.5

O2—P1—O3	115.1 (6)	C15—C14—N6	109.0 (14)
O3—P1—O5	109.3 (5)	C15—C14—H14	125.5
O3—P1—O4	113.2 (6)	C15—C16—C17	112.4 (14)
C8—O5—P1	122.4 (10)	C15—C16—H16A	109.1
P1—O4—H4	109.5	C15—C16—H16B	109.1
C14—N6—H6	124.9	C17—C16—H16A	109.1
C10—N6—H6	124.9	C17—C16—H16B	109.1
C10—N6—C14	110.2 (14)	H16A—C16—H16B	107.9
C17—N7—H7	108.1	C8—C13—H13	120.8
C17—N7—C19	110.3 (11)	C12—C13—C8	118.4 (16)
C18—N7—H7	108.1	C12—C13—H13	120.8
C18—N7—C17	111.4 (11)	N7—C18—H18A	109.5
C18—N7—C19	110.8 (11)	N7—C18—H18B	109.5
C19—N7—H7	108.1	N7—C18—H18C	109.5
C9—C15—C16	128.1 (17)	H18A—C18—H18B	109.5
C14—C15—C9	106.0 (15)	H18A—C18—H18C	109.5
C14—C15—C16	125.7 (17)	H18B—C18—H18C	109.5
C9—C8—O5	118.6 (18)	N7—C19—H19A	109.5
C9—C8—C13	122.2 (16)	N7—C19—H19B	109.5
C13—C8—O5	119.0 (16)	N7—C19—H19C	109.5
C8—C9—C15	135.8 (19)	H19A—C19—H19B	109.5
C8—C9—C10	115.6 (18)	H19A—C19—H19C	109.5
C10—C9—C15	108.6 (16)	H19B—C19—H19C	109.5
N7—C17—H17A	109.1	C11—C12—H12	118.4
N7—C17—H17B	109.1	C13—C12—C11	123.1 (16)
N7—C17—C16	112.7 (12)	C13—C12—H12	118.4
H17A—C17—H17B	107.8	N6—C10—C9	106.2 (17)
C16—C17—H17A	109.1	N6—C10—C11	127.8 (19)
C16—C17—H17B	109.1	C11—C10—C9	125.9 (18)
C12—C11—H11	122.8		

P1—O5—C8—C9	129.3 (13)	C14—N6—C10—C9	−0.5 (17)
P1—O5—C8—C13	−56.5 (17)	C14—N6—C10—C11	176.4 (15)
O5—C8—C9—C15	−4 (3)	C14—C15—C9—C8	177.8 (18)
O5—C8—C9—C10	174.3 (13)	C14—C15—C9—C10	−0.3 (18)
O5—C8—C13—C12	−179.3 (13)	C14—C15—C16—C17	109.3 (17)
O4—P1—O5—C8	−176.8 (11)	C16—C15—C9—C8	−8 (3)
O2—P1—O5—C8	−62.6 (12)	C16—C15—C9—C10	173.7 (16)
O3—P1—O5—C8	63.7 (12)	C16—C15—C14—N6	−174.3 (15)
N7—C17—C16—C15	176.8 (12)	C13—C8—C9—C15	−177.7 (17)
C15—C9—C10—N6	0.5 (18)	C13—C8—C9—C10	0 (2)
C15—C9—C10—C11	−176.4 (15)	C18—N7—C17—C16	−149.7 (12)
C8—C9—C10—N6	−178.0 (13)	C19—N7—C17—C16	86.8 (14)
C8—C9—C10—C11	5 (2)	C12—C11—C10—N6	179.0 (15)
C8—C13—C12—C11	6 (2)	C12—C11—C10—C9	−5 (2)
C9—C15—C14—N6	0.0 (17)	C10—N6—C14—C15	0.4 (17)
C9—C15—C16—C17	−64 (2)	C10—C11—C12—C13	−1 (2)
C9—C8—C13—C12	−5 (2)		

3-[2-(Dimethylamino)ethyl]-1*H*-indol-4-yl dihydrogen phosphate trihydrate (ps1_100k_hydrate_recryst_auto)

Crystal data

$C_{12}H_{17}N_2O_4P·3H_2O$
$M_r = 338.29$
Orthorhombic, *Pbca*
$a = 14.3405$ (6) Å
$b = 8.2707$ (3) Å
$c = 27.098$ (1) Å
$V = 3214.0$ (2) Å^3
$Z = 8$
$F(000) = 1440$
$D_x = 1.398$ Mg m^{-3}
Cu $K\alpha$ radiation, $\lambda = 1.54184$ Å
Cell parameters from 2310 reflections
$\theta = 3.3–73.3°$
$\mu = 1.85$ mm^{-1}
$T = 100$ K
Block, clear light colourless
0.13 × 0.05 × 0.04 mm

Data collection

XtaLAB Synergy, Single source at home/near, HyPix diffractometer
Radiation source: micro-focus sealed X-ray tube, PhotonJet (Cu) X-ray Source
Mirror monochromator
Detector resolution: 10.0000 pixels mm^{-1}
ω scans
Absorption correction: multi-scan (CrysAlis PRO; Rigaku OD, 2024)
$T_{min} = 0.615$, $T_{max} = 1.000$
12268 measured reflections
3256 independent reflections
2382 reflections with $I > 2\sigma(I)$
$R_{int} = 0.091$
$\theta_{max} = 79.3°$, $\theta_{min} = 3.3°$
$h = -15\rightarrow18$
$k = -6\rightarrow10$
$l = -34\rightarrow34$

Refinement

Refinement on F^2
Least-squares matrix: full
$R[F^2 > 2\sigma(F^2)] = 0.052$
$wR(F^2) = 0.120$
$S = 1.04$
3256 reflections
211 parameters
0 restraints
Hydrogen site location: mixed
H-atom parameters constrained
$w = 1/[\sigma^2(F_o^2) + (0.0178P)^2 + 3.4248P]$ where $P = (F_o^2 + 2F_c^2)/3$
$(\Delta/\sigma)_{max} = 0.001$
$\Delta\rho_{max} = 0.36$ e Å^{-3}
$\Delta\rho_{min} = -0.48$ e Å^{-3}

Special details

Geometry. All e.s.d.'s (except the e.s.d. in the dihedral angle between two l.s. planes) are estimated using the full covariance matrix. The cell e.s.d.'s are taken into account individually in the estimation of e.s.d.'s in distances, angles and torsion angles; correlations between e.s.d.'s in cell parameters are only used when they are defined by crystal symmetry. An approximate (isotropic) treatment of cell e.s.d.'s is used for estimating e.s.d.'s involving l.s. planes.

Fractional atomic coordinates and isotropic or equivalent isotropic displacement parameters (Å²)

	x	*y*	*z*	U_{iso}*/U_{eq}
P1	0.92494 (5)	0.36117 (8)	0.55230 (2)	0.01156 (16)
O5	0.90092 (13)	0.4647 (2)	0.60101 (6)	0.0128 (4)
O2	0.88834 (15)	0.1936 (2)	0.55872 (7)	0.0159 (4)
O4	1.03363 (13)	0.3565 (2)	0.54911 (7)	0.0170 (4)
H4	1.051771	0.419918	0.526881	0.025*
O3	0.88452 (14)	0.4585 (2)	0.51054 (7)	0.0168 (4)
O7	0.71249 (15)	0.1728 (3)	0.40288 (7)	0.0212 (4)
H7A	0.655669	0.177781	0.414046	0.032*
H7B	0.745799	0.145864	0.428469	0.032*

O6	0.79746 (16)	0.0341 (3)	0.48255 (7)	0.0246 (5)
H6A	0.818913	0.099334	0.505045	0.037*
H6B	0.745419	−0.002182	0.494787	0.037*
O8	0.77588 (19)	0.4082 (3)	0.33838 (8)	0.0305 (6)
H8A	0.758593	0.334819	0.359436	0.046*
H8B	0.779033	0.496851	0.355568	0.046*
N7	0.53409 (16)	0.4368 (3)	0.60186 (8)	0.0131 (5)
H7	0.565556	0.537578	0.590092	0.016*
N6	0.79851 (17)	0.1754 (3)	0.73888 (8)	0.0154 (5)
H6	0.795486	0.123080	0.767115	0.019*
C10	0.8761 (2)	0.2495 (3)	0.71985 (10)	0.0143 (6)
C17	0.59537 (19)	0.3618 (3)	0.63999 (9)	0.0147 (5)
H17A	0.568600	0.256214	0.649719	0.018*
H17B	0.595896	0.431933	0.669608	0.018*
C11	0.9655 (2)	0.2661 (3)	0.74049 (10)	0.0177 (6)
H11	0.980436	0.219930	0.771597	0.021*
C8	0.9215 (2)	0.3970 (3)	0.64722 (9)	0.0131 (5)
C14	0.7266 (2)	0.1968 (3)	0.70634 (9)	0.0147 (5)
H14	0.664951	0.158289	0.711478	0.018*
C16	0.6951 (2)	0.3361 (3)	0.62286 (9)	0.0149 (5)
H16A	0.696455	0.253806	0.596333	0.018*
H16B	0.720295	0.438359	0.609346	0.018*
C15	0.7548 (2)	0.2806 (3)	0.66548 (9)	0.0125 (5)
C9	0.8520 (2)	0.3144 (3)	0.67336 (9)	0.0119 (5)
C13	1.0091 (2)	0.4174 (3)	0.66692 (10)	0.0169 (6)
H13	1.055240	0.475451	0.649032	0.020*
C18	0.5192 (2)	0.3308 (3)	0.55809 (10)	0.0195 (6)
H18A	0.579514	0.304628	0.543093	0.029*
H18B	0.480071	0.387163	0.533947	0.029*
H18C	0.488182	0.230795	0.568466	0.029*
C12	1.0306 (2)	0.3518 (4)	0.71395 (10)	0.0183 (6)
H12	1.091200	0.367327	0.727354	0.022*
C19	0.4430 (2)	0.4847 (4)	0.62373 (11)	0.0201 (6)
H19A	0.410567	0.388208	0.635864	0.030*
H19B	0.404701	0.537776	0.598526	0.030*
H19C	0.453626	0.559512	0.651189	0.030*

Atomic displacement parameters (Å²)

	U^{11}	U^{22}	U^{33}	U^{12}	U^{13}	U^{23}
P1	0.0136 (3)	0.0101 (3)	0.0110 (3)	0.0003 (3)	0.0000 (2)	0.0022 (2)
O5	0.0163 (9)	0.0099 (9)	0.0123 (8)	0.0019 (7)	0.0011 (7)	0.0031 (7)
O2	0.0244 (10)	0.0094 (9)	0.0140 (9)	−0.0014 (8)	−0.0017 (8)	0.0018 (7)
O4	0.0170 (9)	0.0196 (10)	0.0144 (8)	0.0006 (8)	0.0023 (8)	0.0069 (8)
O3	0.0160 (9)	0.0188 (10)	0.0156 (9)	0.0011 (8)	−0.0014 (8)	0.0047 (8)
O7	0.0223 (10)	0.0233 (11)	0.0181 (9)	0.0019 (9)	0.0035 (8)	−0.0001 (8)
O6	0.0227 (11)	0.0324 (13)	0.0186 (10)	−0.0100 (10)	0.0011 (9)	−0.0028 (9)
O8	0.0466 (15)	0.0281 (12)	0.0167 (10)	−0.0144 (11)	0.0107 (10)	−0.0068 (9)

N7	0.0181 (11)	0.0090 (11)	0.0122 (10)	−0.0001 (9)	−0.0014 (9)	0.0002 (8)
N6	0.0212 (12)	0.0134 (12)	0.0118 (10)	0.0015 (10)	0.0006 (9)	0.0028 (8)
C10	0.0218 (15)	0.0089 (12)	0.0123 (12)	0.0002 (11)	0.0014 (10)	−0.0019 (9)
C17	0.0182 (14)	0.0120 (13)	0.0137 (11)	0.0014 (11)	0.0000 (10)	0.0016 (10)
C11	0.0266 (16)	0.0153 (14)	0.0112 (11)	−0.0003 (12)	−0.0028 (11)	−0.0011 (10)
C8	0.0201 (13)	0.0090 (13)	0.0103 (11)	0.0018 (11)	0.0019 (10)	−0.0003 (9)
C14	0.0165 (13)	0.0142 (14)	0.0134 (11)	−0.0011 (11)	0.0029 (10)	−0.0009 (10)
C16	0.0173 (13)	0.0137 (14)	0.0136 (11)	−0.0034 (11)	−0.0016 (10)	0.0001 (10)
C15	0.0175 (13)	0.0080 (13)	0.0119 (11)	0.0010 (10)	0.0015 (10)	0.0000 (9)
C9	0.0170 (13)	0.0070 (12)	0.0116 (11)	0.0021 (10)	−0.0003 (10)	−0.0027 (9)
C13	0.0214 (14)	0.0126 (14)	0.0166 (12)	−0.0020 (11)	−0.0010 (11)	−0.0023 (10)
C18	0.0252 (15)	0.0153 (14)	0.0178 (13)	0.0033 (12)	−0.0060 (11)	−0.0037 (11)
C12	0.0188 (13)	0.0172 (14)	0.0190 (12)	0.0004 (12)	−0.0060 (11)	−0.0033 (11)
C19	0.0183 (14)	0.0161 (15)	0.0260 (14)	0.0037 (12)	0.0003 (11)	−0.0005 (12)

Geometric parameters (Å, º)

P1—O5	1.6107 (19)	C17—H17B	0.9900
P1—O2	1.492 (2)	C17—C16	1.519 (4)
P1—O4	1.562 (2)	C11—H11	0.9500
P1—O3	1.5047 (19)	C11—C12	1.375 (4)
O5—C8	1.403 (3)	C8—C9	1.401 (4)
O4—H4	0.8400	C8—C13	1.376 (4)
O7—H7A	0.8702	C14—H14	0.9500
O7—H7B	0.8709	C14—C15	1.368 (4)
O6—H6A	0.8700	C16—H16A	0.9900
O6—H6B	0.8701	C16—H16B	0.9900
O8—H8A	0.8694	C16—C15	1.509 (4)
O8—H8B	0.8695	C15—C9	1.437 (4)
N7—H7	1.0000	C13—H13	0.9500
N7—C17	1.492 (3)	C13—C12	1.419 (4)
N7—C18	1.490 (3)	C18—H18A	0.9800
N7—C19	1.488 (4)	C18—H18B	0.9800
N6—H6	0.8800	C18—H18C	0.9800
N6—C10	1.371 (4)	C12—H12	0.9500
N6—C14	1.368 (4)	C19—H19A	0.9800
C10—C11	1.406 (4)	C19—H19B	0.9800
C10—C9	1.412 (4)	C19—H19C	0.9800
C17—H17A	0.9900		

O2—P1—O5	108.85 (11)	C13—C8—C9	120.9 (2)
O2—P1—O4	109.55 (12)	N6—C14—H14	124.3
O2—P1—O3	116.67 (11)	C15—C14—N6	111.4 (3)
O4—P1—O5	105.78 (11)	C15—C14—H14	124.3
O3—P1—O5	104.46 (10)	C17—C16—H16A	109.6
O3—P1—O4	110.86 (11)	C17—C16—H16B	109.6
C8—O5—P1	118.29 (16)	H16A—C16—H16B	108.2
P1—O4—H4	109.5	C15—C16—C17	110.1 (2)

H7A—O7—H7B	104.4	C15—C16—H16A	109.6
H6A—O6—H6B	104.5	C15—C16—H16B	109.6
H8A—O8—H8B	104.6	C14—C15—C16	127.3 (3)
C17—N7—H7	107.5	C14—C15—C9	105.4 (2)
C18—N7—H7	107.5	C9—C15—C16	127.2 (2)
C18—N7—C17	113.0 (2)	C10—C9—C15	107.2 (2)
C19—N7—H7	107.5	C8—C9—C10	117.5 (3)
C19—N7—C17	110.6 (2)	C8—C9—C15	135.2 (2)
C19—N7—C18	110.3 (2)	C8—C13—H13	120.0
C10—N6—H6	125.9	C8—C13—C12	120.0 (3)
C14—N6—H6	125.9	C12—C13—H13	120.0
C14—N6—C10	108.1 (2)	N7—C18—H18A	109.5
N6—C10—C11	129.4 (2)	N7—C18—H18B	109.5
N6—C10—C9	107.9 (2)	N7—C18—H18C	109.5
C11—C10—C9	122.7 (3)	H18A—C18—H18B	109.5
N7—C17—H17A	108.8	H18A—C18—H18C	109.5
N7—C17—H17B	108.8	H18B—C18—H18C	109.5
N7—C17—C16	113.7 (2)	C11—C12—C13	121.3 (3)
H17A—C17—H17B	107.7	C11—C12—H12	119.4
C16—C17—H17A	108.8	C13—C12—H12	119.4
C16—C17—H17B	108.8	N7—C19—H19A	109.5
C10—C11—H11	121.2	N7—C19—H19B	109.5
C12—C11—C10	117.5 (2)	N7—C19—H19C	109.5
C12—C11—H11	121.2	H19A—C19—H19B	109.5
C9—C8—O5	119.8 (2)	H19A—C19—H19C	109.5
C13—C8—O5	119.3 (2)	H19B—C19—H19C	109.5

P1—O5—C8—C9	−95.4 (3)	C17—C16—C15—C9	−147.8 (3)
P1—O5—C8—C13	86.7 (3)	C11—C10—C9—C8	0.6 (4)
O5—C8—C9—C10	−179.5 (2)	C11—C10—C9—C15	−177.4 (2)
O5—C8—C9—C15	−2.3 (5)	C8—C13—C12—C11	0.5 (4)
O5—C8—C13—C12	179.0 (2)	C14—N6—C10—C11	177.2 (3)
O2—P1—O5—C8	48.3 (2)	C14—N6—C10—C9	−1.9 (3)
O4—P1—O5—C8	−69.3 (2)	C14—C15—C9—C10	−1.0 (3)
O3—P1—O5—C8	173.60 (19)	C14—C15—C9—C8	−178.4 (3)
N7—C17—C16—C15	172.6 (2)	C16—C15—C9—C10	175.2 (3)
N6—C10—C11—C12	−177.9 (3)	C16—C15—C9—C8	−2.3 (5)
N6—C10—C9—C8	179.7 (2)	C9—C10—C11—C12	1.0 (4)
N6—C10—C9—C15	1.8 (3)	C9—C8—C13—C12	1.2 (4)
N6—C14—C15—C16	−176.3 (2)	C13—C8—C9—C10	−1.7 (4)
N6—C14—C15—C9	−0.2 (3)	C13—C8—C9—C15	175.5 (3)
C10—N6—C14—C15	1.3 (3)	C18—N7—C17—C16	65.6 (3)
C10—C11—C12—C13	−1.6 (4)	C19—N7—C17—C16	−170.1 (2)
C17—C16—C15—C14	27.5 (4)		